Synthesis, sintering and expansion of $Al_{0.8}Mg_{0.6}Ti_{1.6}O_5$: a low-thermal-expansion material resistant to thermal decomposition

V. BUSCAGLIA, F. CARACCIOLO, M. LEONI
Istituto di Chimica Fisica Applicata dei Materiali, Consiglio Nazionale delle Ricerche, via De Marini 6, I-16149 Genoa, Italy

P. NANNI, M. VIVIANI
Istituto di Chimica, Facoltà di Ingegneria, Fiera del Mare, Pad. D, I-16129 Genoa, Italy

J. LEMAITRE
Ecole Polytechnique Fédérale de Lausanne (EPFL), Laboratoire de Technologie des Poudres, MX-Ecublens, CH-1015 Lausanne, Switzerland

A low-thermal-expansion ceramic with the composition $Al_{0.8}Mg_{0.6}Ti_{1.6}O_5$ that is isostructural to aluminium titanate Al_2TiO_5, was prepared by solid-state reaction of a mixture of α-Al_2O_3, MgO and TiO_2-rutile. The synthesized material does not decompose after annealing for 250 h in the temperature range of 900–1175 °C. The ceramic sintered at 1350 °C has a 97% relative density, a grain size of ≈ 5 μm and an average thermal expansion coefficient between 80 and 1000 °C of $\approx 2 \times 10^{-6}\,K^{-1}$. Materials with the same composition, but obtained by reaction sintering, have a higher thermal expansion coefficient ($4 \times 10^{-6}\,K^{-1}$) and showed the presence of secondary phases.

1. Introduction

The development of Al_2TiO_5 based ceramics for applications requiring high thermal shock resistance and good thermal insulation, such as liners and manifolds of internal combustion engines, components exposed to molten metals in metallurgy and thermal barriers, has received a considerable amount of attention in recent years. Sintered aluminium titanate materials, due to a thermal expansion anisotropy of individual grains [1], develop extensive microcracking, generally along grain boundaries, when the grain size increases beyond a critical value [2–5]. The presence of microcracks results in a low apparent thermal expansion ($\alpha_{25-1000} \approx 1 \times 10^{-6}\,K^{-1}$), but also in a poor mechanical strength [6]. The mechanical properties can be improved using composite materials obtained by reaction sintering: Al_2TiO_5–mullite [7], Al_2TiO_5–$ZrTiO_4$–ZrO_2 [8], Al_2TiO_5–mullite–ZrO_2 [9]. A serious limitation to practical application of Al_2TiO_5 is also related to the thermal instability of this material, which decomposes to Al_2O_3 and TiO_2 below 1280 °C [10]. The decomposition of aluminium titanate can be controlled by MgO or Fe_2O_3 addition [11, 12], which leads to the formation of solid solutions between Al_2TiO_5 and the isostructural compounds $MgTi_2O_5$($Al_{2(1-x)}Mg_xTi_{(1+x)}O_5$) and Fe_2TiO_5 ($Al_{2(1-x)}Fe_{2x}TiO_5$) during sintering. However, limited addition (10–20 mol %), does not provide long term stability in the temperature range of 1000–1100 °C, but only a delay before the decomposition starts [9, 11]. The decomposition follows a nucleation and growth mechanism and proceeds quickly after an initial incubation period [13, 14]. In a recent paper, a systematic investigation of the decomposition of Al_2TiO_5 containing 0, 10, 20, 40, 50 and 60 mol % $MgTi_2O_5$ was presented [15]. Only the solid solution containing 60 mol % $MgTi_2O_5$ which corresponds to the composition $Al_{0.8}Mg_{0.6}Ti_{1.6}O_5$ was unaffected by decomposition after 250 h of annealing at different temperatures in the range of 900–1175 °C. A research programme on the properties of ceramics with this composition has been undertaken in order to define potential technological applications.

In this paper, the synthesis and sintering of $Al_{0.8}Mg_{0.6}Ti_{1.6}O_5$ powders obtained by different solid-state routes, as well as the thermal expansion of the final material, are presented.

2. Experimental procedure

The powders used in the sintering process were prepared from stoichiometric quantities of α-Al_2O_3 (Baikowski CR6, 99.99%, $X_{50} = 0.5$ μm), TiO_2 (Aldrich 1317-80-2, predominantly rutile, 99.9%, $X_{50} =$ 1 μm) and MgO (Aldrich 34279-3, 99%). The mixture was wet-milled in water for 24 h with alumina balls inside polyethylene bottles. Three different powders were obtained by different thermal treatments: (i) the as-prepared mixture (M6); (ii) 2 h firing at 1100 °C

0022–2461

(M611) and (iii) 2 h firing at 1300 °C (M613). These conditions were chosen to have different levels of reaction at the sintering stage. The M6 series corresponds to a completely unreacted powder, M611 to a partially reacted powder and M613 to a completely transformed powder. The powders M611 and M613, after high-temperature firing, were again wet milled in water for 24 h. After drying and sieving, green bodies (cylinders of ≈ 1 cm diameter and ≈ 10 cm in length) were prepared by cold isostatic pressing at 150 MPa.

The formation of the Al_2TiO_5–$MgTi_2O_5$ solid solution was studied on M6 loose powders at 1000, 1100, 1200 and 1300 °C for times ranging from 0.5 to 7 h. The samples were placed inside the furnace and they reached the reaction temperature within 2–3 min. At the end of the reaction time the samples were removed from the furnace and air-quenched. The phases present after the reaction were detected by X-ray diffraction (XRD, Philips PW1710, Co K_α radiation, graphite monochromator). The lattice parameters of the main reaction product, the solid solution Al_2TiO_5– $MgTi_2O_5$, were determined without the use of an internal standard by using a least squares procedure and allowing numerical correction for possible sample displacement. The composition (x in $Al_{2(1-x)}Mg_xTi_{(1+x)}O_5$) of the solid solution as a function of time was calculated from the value of the lattice constants using a calibration line derived from a series of single-phase standards (x = 0, 0.1, 0.2, 0.4, 0.5, 0.6, 0.8, 1.0). The absolute average error on the calculated compositions is ± 0.02. A semi-quantitative evaluation of the phase composition of the reacted powders was obtained using the Rietveld method as implemented in the DBWS program [16]. All calculations were performed using the software Cerius^2 developed by BIOSYM/Molecular Simulations.

The shrinkage behaviour of the different powders was studied from room temperature up to 1500 °C, with a constant heating rate of 1 °C min^{-1}, using a dilatometer (Setaram DHT).

Green bodies were sintered in a box furnace heated by SuperKanthal elements (Lindberg) at 1300, 1350, 1400, 1450 and 1500 °C. The sintering times were 2 and 4 h at 1300 °C and 2 h at the higher temperatures. The heating rate was 1 °C min^{-1}. An isothermal treatment at 300 °C for 5 h during heating allowed for the removal of the organic additives (PAA and polysaccharide). The density of the sintered materials was measured by immersion in water, after the samples had been coated with a thin gloss layer to avoid water absorption. The sample microstructure was observed by scanning electron microscopy (SEM, Philips 515), after metallographic preparation and thermal etching of the specimens. The presence of secondary phases was studied by XRD after grinding in an agate mortar.

The expansion of the sintered samples between room temperature and 1000 °C during both heating and cooling was also measured using the dilatometer (Setaram DHT) at a constant heating and cooling rate of 2 °C min^{-1}.

3. Results and discussion

3.1. Solid state reactions

The phases detected after powder reaction were the solid solution $Al_{2(1-x)}Mg_xTi_{(1+x)}O_5$, $MgAl_2O_4$, TiO_2-rutile and α-Al_2O_3. In powders reacted at 1000 °C for 0.5 and 1 h a small amount of $MgTiO_3$ was also found. Even though the solid solution with x = 0.6 probably represents the equilibrium state of the system in the investigated temperature range [15], from the kinetic point of view its formation occurs by different steps. The composition of the reacted samples at the different temperatures is shown in Fig. 1(a–d). Error bars are not reported as the plotted values represent only a semi-quantitative estimation, but the observed trends are representative of the phase composition evolution. In any case, the main reaction product was the titanate solid solution with composition ranging from $x \cong 1$ to x = 0.6, depending on the temperature and reaction time, as shown in Fig. 2. The $MgTi_2O_5$ phase forms very rapidly at the beginning of the reaction, even at 1000 °C, according to the reaction:

$$MgO + 2TiO_2 \rightarrow MgTi_2O_5 \quad (1)$$

with complete conversion of the MgO present in the mixture. It should be noted that the reaction shown as Equation 1 only represents the overall $MgTi_2O_5$ formation process, which probably occurs in various steps. A possible mechanism involves the formation of the intermediate phases Mg_2TiO_4 and $MgTiO_3$, as suggested by the phase diagram of the MgO–TiO_2 system [17]. The small amount of $MgTiO_3$ present after a 0.5 h reaction at 1000 °C transforms in $MgTi_2O_5$ by the reaction:

$$MgTiO_3 + TiO_2 \rightarrow MgTi_2O_5 \quad (2)$$

as can be argued by the simultaneous decrease of the TiO_2 weight fraction. The Gibbs free energy of the reaction shown as Equation 2 is negative at temperatures above 628 °C [18]. Only a limited amount of Al_2TiO_5 (5–8 wt %) enters into the solid solution at 1000 °C and the composition remains almost constant after a 1 h reaction. At higher temperatures, the solid solution gradually enriches in Al_2TiO_5 as the reaction time increases to approach the final composition of x = 0.6. The transformation of the parent oxides into $Al_{0.8}Mg_{0.6}Ti_{1.6}O_5$ is almost completed after 7 h at 1300 °C. The formation of Al_2TiO_5 in solid solution with $MgTi_2O_5$ occurs by conversion of the residual Al_2O_3 and TiO_2 particles dispersed in the $MgTi_2O_5$-rich solid solution matrix already formed according to:

$$Al_2O_3 + TiO_2 \rightarrow [Al_2TiO_5] \quad (3)$$

where the square bracket indicates the existence of the phase at an activity less than one, i.e., in solid solution. However, reaction 3 is quite slow in comparison with reaction 1 and has to occur by solid state diffusion through the $MgTi_2O_5$ matrix. Four different mechanisms are possible: counterdiffusion of Al^{3+} and Ti^{4+}, parallel diffusion of Al^{3+} and O^{2-}, parallel diffusion of Ti^{4+} and O^{2-}, parallel diffusion of the faster

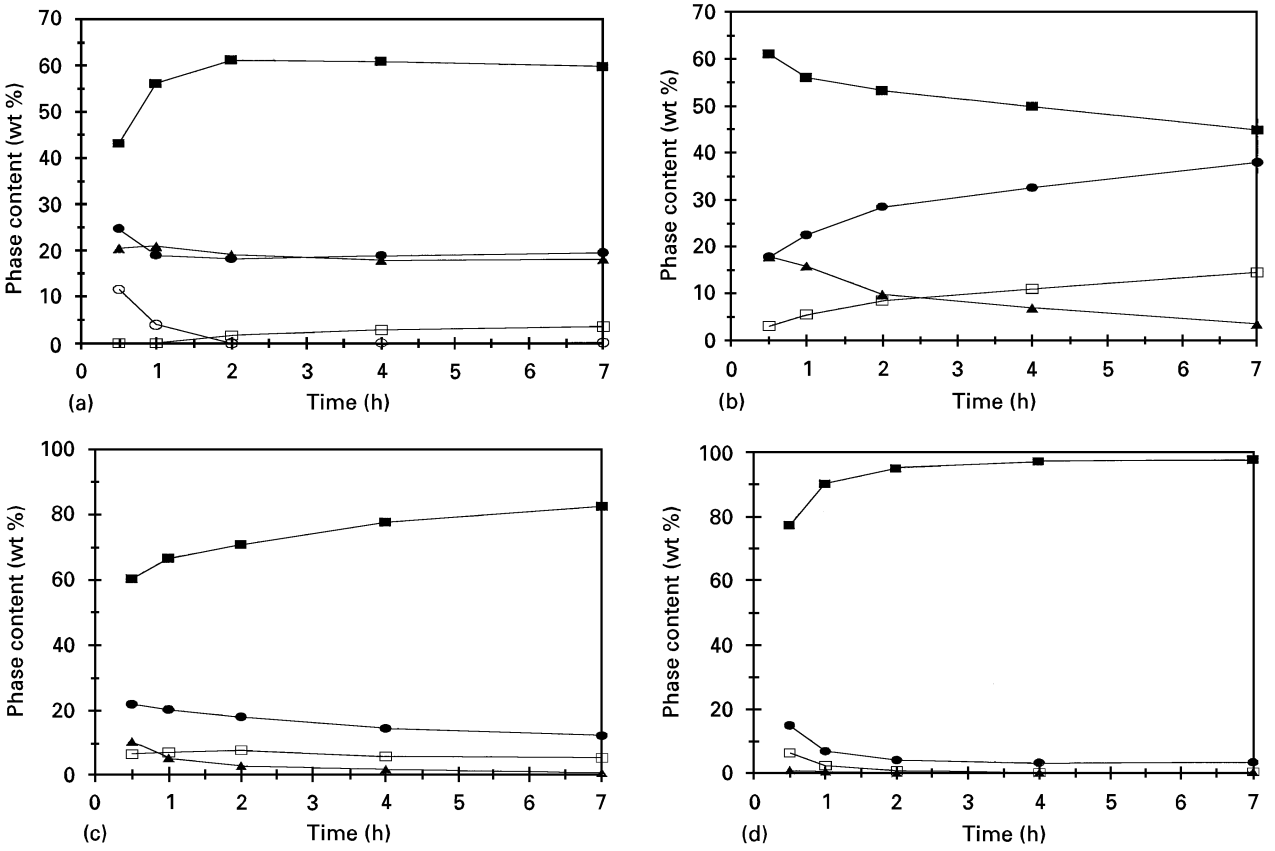

Figure 1 Weight fraction as a function of time of phases present during the solid-state reaction between MgO, TiO_2-rutile and α-Al_2O_3; (■) $Al_{2(1-x)}Mg_xTi_{(1+x)}O_5$ solid solution; (●) TiO_2-rutile; (▲) α-Al_2O_3; (□) $MgAl_2O_4$ and (○) $MgTiO_3$ (a) 1000 °C; (b) 1100 °C, (c) 1200 °C and (d) 1300 °C.

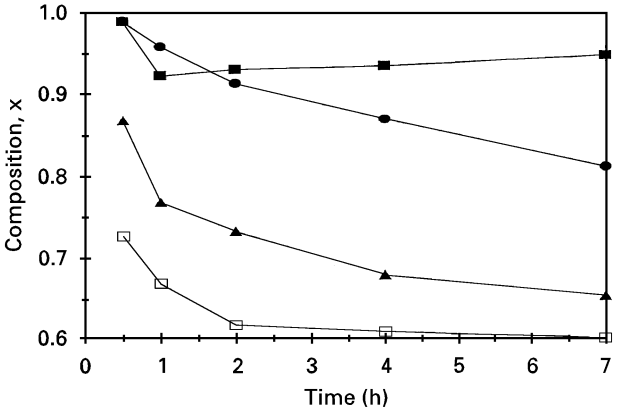

Figure 2 Composition x, of the solid solution $Al_{2(1-x)}Mg_xTi_{(1+x)}O_5$ resulting from solid-state reaction between MgO, TiO_2-rutile and α-Al_2O_3 (■) 1000 °C; (●) 1100 °C; (▲) 1200 °C; (□) 1300 °C.

moving cation and electrons coupled with oxygen transport in the gas phase. A similar behaviour was observed for the formation of Al_2TiO_5 in alumina–titania mixtures [19]: the conversion of particles trapped in the reaction product is two orders of magnitude slower than the initial formation of aluminium titanate. The reaction is probably controlled, in both cases, by the slow diffusion of Al^{3+} or Ti^{4+} ions in the titanate matrix. In addition, the coarsening of Al_2O_3 and TiO_2 particles related to Ostwald ripening contributes in slowing down the kinetics. Owing to the slowness of reaction 3, other processes can be promoted. The formation of a spinel at 1000 °C and, in particular, at 1100 °C occurs by the reaction:

$$MgTi_2O_5 + Al_2O_3 \rightarrow MgAl_2O_4 + 2TiO_2 \quad (4)$$

whose Gibbs free energy is significantly negative [18]. This is a consequence of the higher thermodynamic stability of $MgAl_2O_4$ in comparison with the other ternary phases present in the Al_2O_3–TiO_2–MgO system, as indicated by the available thermochemical data [18]. Therefore, when any kind of magnesium titanate ($MgTiO_3$, Mg_2TiO_4 and $MgTi_2O_5$) is placed in contact with alumina, it spontaneously transforms into spinel and rutile, as shown in Fig. 3. The occurrence of reaction 4 has already been discussed in a previous paper [20].

3.2. Dynamic sintering

Different processes are expected to occur during the constant-heating-rate sintering of the powders. In particular, the reaction between the parent oxides will occur in the M6 samples whereas the solid solution already present in the M611 samples will enrich in Al_2TiO_5. Only sintering will take place for the M613 samples as the formation of the solid solution is almost already completed in the powders.

The expansion and expansion rate as a function of temperature of an M6 green body is shown in Fig. 4. Three sharp peaks in the expansion rate are present: two expansion peaks (949 and 1219 °C) and one shrinkage peak (1372 °C). The first expansion peak corresponds to the formation of $MgTi_2O_5$ through

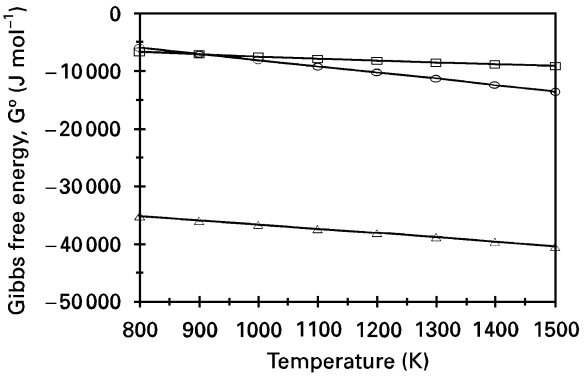

Figure 3 Standard Gibbs free energy as a function of temperature for the following reactions: (□) $MgTi_2O_5 + Al_2O_3 \rightarrow MgAl_2O_4 + 2TiO_2$; (○) $MgTiO_3 + Al_2O_3 \rightarrow MgAl_2O_4 + TiO_2$; (△) $Mg_2TiO_4 + 2Al_2O_3 \rightarrow 2MgAl_2O_4 + TiO_2$.

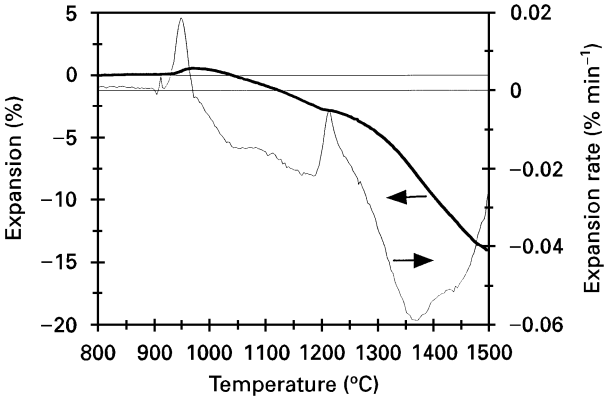

Figure 4 Expansion and expansion rate of a green body from the M6-series.

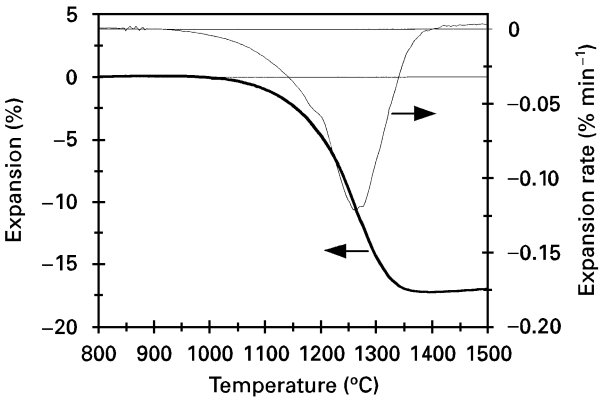

Figure 5 Expansion and expansion rate of a green body from the M611-series.

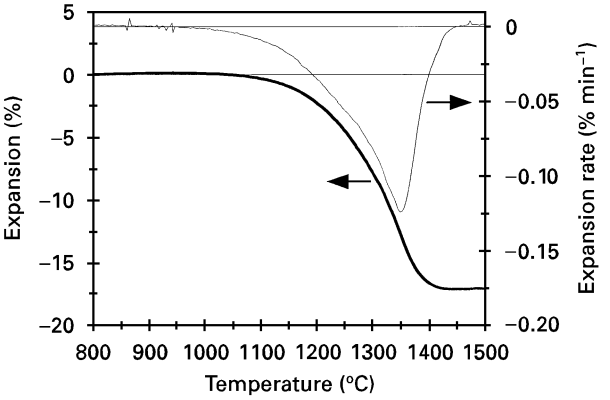

Figure 6 Expansion and expansion rate of a green body from the M613-series.

reaction 1, whereas the second one is related to the formation of Al_2TiO_5 through reaction 3. Both reactions proceed with an increase in volume, as the density of $MgTi_2O_5$ (3.65 g cm^{-3}) as well as that of Al_2TiO_5 (3.7 g cm^{-3}) is lower than the average density of the parent oxides (4.1 g cm^{-3} for both $MgO + 2\,TiO_2$ and $Al_2O_3 + TiO_2$). For the second peak, the expansion is partly balanced by the shrinkage associated with the sintering of the matrix and there is no net volume increase. The third peak corresponds to the sintering of the titanate solid solution.

The expansion and expansion rate as a function of temperature of the M611 and M613 samples are shown in Figs 5 and 6, respectively. The two powders have the same sintering behaviour except for the position of the maximum sintering rate: 1263 °C for M611, 1349 °C for M613. The expected expansion related to the formation of Al_2TiO_5 from residual Al_2O_3 and TiO_2 is not observed for sample M611 as the reaction is quite slow and had already partially occurred during the firing stage. In addition, sintering of the matrix is already fast at temperatures around 1200 °C and the corresponding shrinkage effect can hide a small expansion. The sintering rate of the M611 and M613 samples above 1250 °C is in any case much higher than that of the M6 sample. Shrinkage stops at $\approx$ 1400 °C for the M611 samples and $\approx$ 1450 °C for the M613 samples. On the contrary, for the M6 samples, densification continues at higher temperatures and the final shrinkage (13%) is smaller than that observed for the M611 and M613 samples (17.5%). The different sintering behaviour of the M6 powder can be related to the processing conditions: titanate particles directly produced *in situ* by solid-state reaction are likely to have a larger size and to be strongly aggregated in comparison with the M611 and M613 powders which underwent a grinding treatment after firing. However, a better understanding of the densification-reaction history of the M6 powder would require further investigation. In particular, a plot of the apparent density versus the weight fraction of solid solution could be useful to visualize the relative progress of the two concurrent processes (reaction and sintering).

3.3. Microstructure and phase composition

The relative densities of the different samples sintered for 2 and 4 h at 1300 °C and for 2 h at 1350, 1400, 1450 and 1500 °C are reported in Table I. The theoretical density of $Al_{0.8}Mg_{0.6}Ti_{1.6}O_5$ obtained from the unit cell parameters measured by XRD (3.65 g cm^{-3}) was taken as a reference. At 1300 °C there is an increase of the final density by doubling the sintering time, which is particularly remarkable for the M613 powder. The M6 sample has a lower density than the M611 and

TABLE I Relative density (%) of samples sintered at different temperatures

Sample	Temperature (°C)					
	1300 – 2 h	1300 – 4 h	1350 – 2 h	1400 – 2 h	1450 – 2 h	1500 – 2 h
M6	77	80	93	95	95	97
M611	95	99	99	98	97	97
M613	78	97	97	96	96	96

M613 samples for temperatures $< 1500\,^{\circ}C$, in agreement with the dynamic sintering results. Secondary phases, TiO_2-rutile, α-Al_2O_3 and $MgAl_2O_4$- spinel, were detected by XRD in the M6 and M611 samples sintered at 1300, 1350 and 1400 °C. The M6 sample sintered at 1350 °C contained ≈ 4 wt % Al_2O_3 and ≈ 4 wt % TiO_2, whereas the M611 sample contained ≈ 5 wt % TiO_2, ≈ 2 wt % $MgAl_2O_4$ and ≈ 1 wt % Al_2O_3. Rutile and spinel were present as isolated dispersed particles, but the alumina formed small aggregates inside the sintered matrix. These aggregates are probably formed during the mixing of the initial oxides and further slow down the complete transformation of unreacted oxides in the titanate solid solution. The M613 sample contained only traces of TiO_2 (< 1 wt %). The microstructure of the M6, M611 and M613 samples sintered for 2 h at 1350 °C are compared in Figs 7–9. The grains are almost equiaxed in all cases. The faceted small prismatic crystals present in the M6 and M611 samples correspond to unreacted TiO_2. The presence of some multigrain microcracks, often transgranular rather than intergranular, is clearly evident in Figs 7–9. This is an important difference in comparison to ceramics containing a lower amount of magnesium oxide. Solid solutions with $x = 0.1$ and 0.2 prepared from the same raw materials show predominantly intergranular microcracks, in agreement with microstructural observations reported in the literature [2, 3, 8]. The reasons for this different behaviour are currently not clear. The microcracks are formed as the result of the thermal expansion anisotropy of the pseudobrookite structure and are responsible for the low thermal expansion of the material. The average grain size of the different ceramics, expressed as mean intercept length, are reported in Table II. For temperatures $\geqslant 1400\,^{\circ}C$ both normal and exaggerated grain growth occur. The abnormally grown grains present an aspect ratio ranging from 2.5 to 5.5 and could correspond to either elongated or tabular crystals. The biggest grains reach a length of 600 μm in the M611 sample sintered at 1500 °C. The bimodal distribution of grains is shown in Fig. 10 for the M613 powder sintered for 2 h at 1400 °C. Exaggerated grain growth is probably related to the formation of small quantities of liquid or glassy phase due to the presence of silicon impurities in the starting powders (≈ 1000 p.p.m. SiO_2) with preferential growth of some grains. The formation of liquid or glassy phases in the MgO–SiO_2–Al_2O_3 system begins to occur at temperatures slightly above 1350 °C [17]. The abnormal grain growth can be inhibited by the presence of second phase particles located at grain boundaries and/or at triple junctions. The addition of a 10 wt % excess of Al_2O_3 to the solid solutions

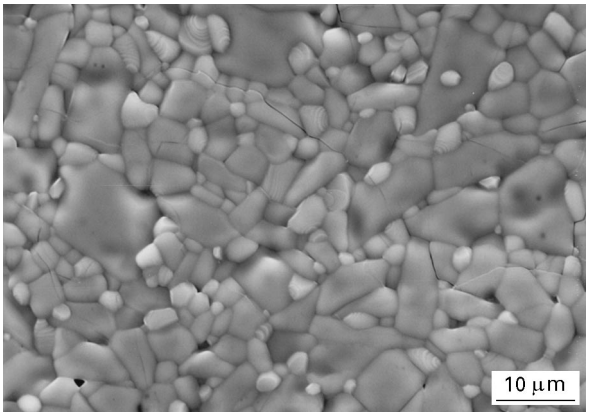

Figure 7 Microstructure of a sample from the M6-series sintered 2 h at 1350 °C (thermally etched, bar = 10 μm).

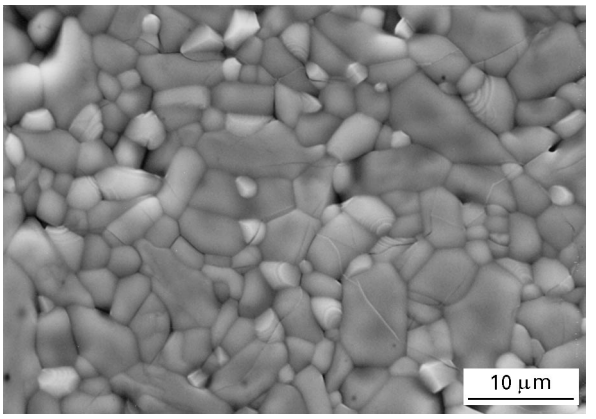

Figure 8 Microstructure of a sample from the M611-series sintered 2 h at 1350 °C (thermally etched, bar = 10 μm).

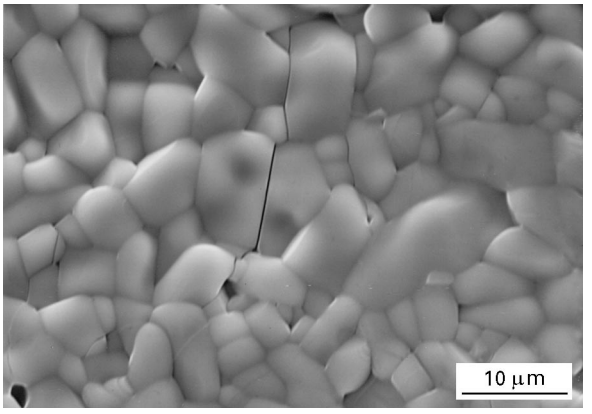

Figure 9 Microstructure of a sample from the M613-series sintered 2 h at 1350 °C (thermally etched, bar = 10 μm).

TABLE II Average grain size (μm) of samples sintered for 2 h at different temperatures

Sample	Temperature (°C)			
	1300 – 2 h	1350 – 2 h	1400 – 2 h	1450 – 2 h
M6	3.3 ± 0.3	3.9 ± 0.3	8.9 ± 1 (Matrix) 50–100 (Abnormal grains)	19.4 ± 2 (Matrix) 70–200 (Abnormal grains)
M611	4.2 ± 0.3	4.2 ± 0.3	13.1 ± 1.5 (Matrix) 50–250 (Abnormal grains)	23.0 ± 2.8 (Matrix) 100–500 (Abnormal grains)
M613	3.3 ± 0.4	5.2 ± 0.4	8.8 ± 0.7 (Matrix) 100–300 (Abnormal grains)	25.0 ± 2.2 (Matrix) 150–350 (Abnormal grains)

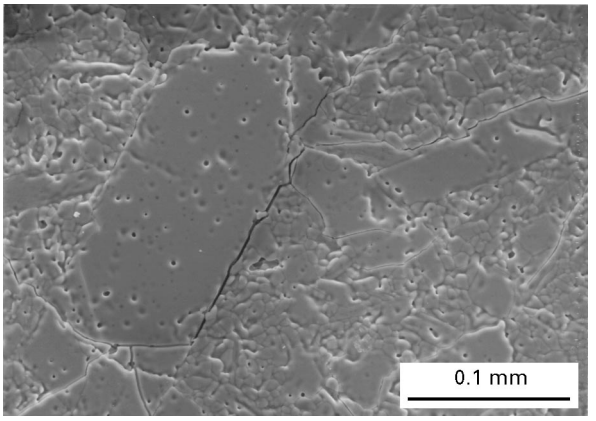

Figure 10 Microstructure of a sample of the M613-series sintered 2 h at 1400 °C (thermally etched, bar = 100 μm).

containing 10 and 20 mol % $MgTi_2O_5$, was completely effective in controlling grain growth [21]. Some experiments are currently in progress to test the effect of alumina on the grain growth of M613 samples.

3.4. Thermal expansion

The thermal expansion behaviours of specimens sintered for 2 h at 1350 °C are reported in Fig. 11(a–c). These materials have a high density with a small grain size without exaggerated grain growth, as indicated by the values reported in Tables I and II. All samples show hysteresis between heating and cooling which is typical of aluminium titanate and, in general, of materials with a pseudobrookite structure. The jagged shape of the heating branch up to ≈ 500 °C is an artefact induced by the temperature controller of the dilatometer furnace. The hysteresis behaviour of the thermal expansion on heating and cooling is evidence for the closing of the microcracks. As is shown in Fig. 11(a–c), a change in the slope of the expansion curve is observed on cooling. Such a change in the slope probably corresponds to the reintroduction of microcracks which starts at ≈ 600 °C for both the M6 and M611 samples and at ≈ 700 °C for the M613

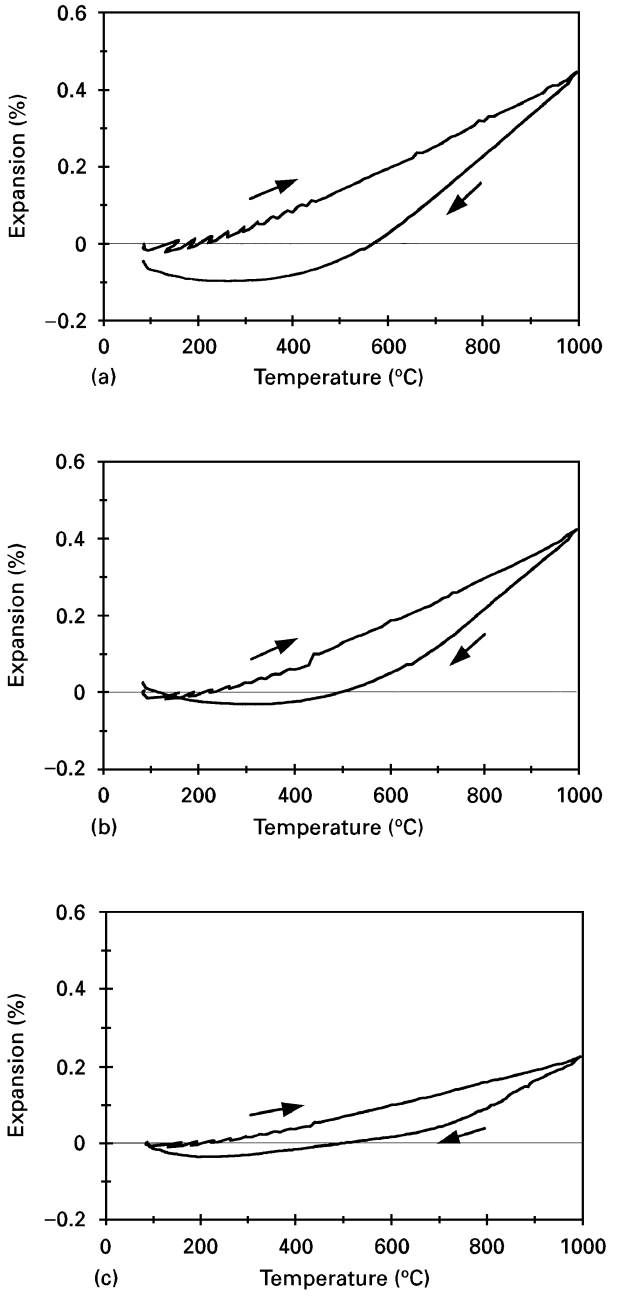

Figure 11 Thermal expansion behaviour of samples heated and cooled from approximately 1000 °C. (a) M6; (b) M611 and (c) M613.

samples. The average value of the thermal expansion coefficient between 80 and 1000 °C is $\approx 4 \times 10^{-6}\,K^{-1}$ for the M6 and M611 samples and $\approx 2 \times 10^{-6}\,K^{-1}$ for the M613 sample. The higher thermal expansion coefficient of the M6 and M611 series in comparison with the M613 sample can be related to the presence of secondary phases and to a smaller grain size (≈ 4 μm for the M6 and M611 and ≈ 5 μm for the M613 samples). The effect of grain size should be dominant as for the present samples it falls in the critical range of 3–8 μm where a rapid transition from low ($0–1 \times 10^{-6}\,K^{-1}$) to higher ($1 \times 10^{-5}\,K^{-1}$) values of the bulk thermal expansion were observed [2–4]. Ohya and Nakagawa have recently established a relationship between the grain size and the grain boundary crack volume [22] and Ohya *et al*. have correlated the crack volume to the thermal expansion coefficient [23]. The application of this model to the present data gives, however, too small values of $\alpha (\approx 1 \times 10^{-7}\,K^{-1}$ for M613 and $\approx 1 \times 10^{-6}\,K^{-1}$ for the M6 and M611 samples). The existence of a stress relaxation mechanism, as observed for a Al_2TiO_5-based ceramic containing 5 wt % MgO [22], can lead to a decrease in the crack volume and, as a consequence, to an increase of the thermal expansion coefficient in comparison to that predicted by the model.

4. Conclusions

The solid solution 40 mol % Al_2TiO_5–60 mol % $MgTi_2O_5$ ($Al_{0.8}Mg_{0.6}Ti_{1.6}O_5$) does not undergo any decomposition after a 250 h annealing in the temperature range of 900–1175 °C, in contrast to solid solutions containing $\leqslant 50$ mol % $MgTi_2O_5$. Single-phase sintered materials with a low thermal expansion coefficient ($\approx 2 \times 10^{-6}\,K^{-1}$) and a small grain size (≈ 5 μm) were obtained by sintering for 2 h at 1350 °C a powder prepared from MgO, TiO_2-rutile and α-Al_2O_3 through a solid-state route. The measured value of the thermal expansion coefficient is comparable to other oxide ceramics, such as standard aluminium titanate ($\approx 1 \times 10^{-6}\,K^{-1}$), porous cordierite ($\approx 1 \times 10^{-6}\,K^{-1}$) and lithium aluminosilicate ($\approx 2 \times 10^{-6}\,K^{-1}$). Ceramic materials with the same composition, but prepared by direct reaction sintering contain secondary phases (TiO_2, Al_2O_3 and $MgAl_2O_4$) and display a higher thermal expansion coefficient ($\approx 4 \times 10^{-6}\,K^{-1}$) due to a smaller grain size (≈ 4 μm). Sintering above 1350 °C results, in any case, in exaggerated grain growth. A better control of the microstructural evolution will enable us to obtain a more reliable ceramic with tailored properties. This goal might be achieved by the development of composite materials. Measurement of the mechanical properties, and in particular of the bending strength, should be undertaken to obtain additional information on the reliability and potential applications of this material.

Acknowledgements

The authors wish to thank Mr C. Bottino for the scanning electron microscopy measurements and Baikowski Chemie-Jocam s.r.l., Milan (Italy), for kindly providing the CR6 alumina powder.

References

1. G. BAYER, *J. Less-Common Metals* **24** (1971) 129.
2. J. J. CLEVELAND and R. C. BRADT, *J. Amer. Ceram. Soc.* **61** (1978) 478.
3. Y. OHYA, Z. NAKAGAWA and K. HAMANO, *ibid.* **70** (1987) C184.
4. F. J. PARKER and R. W. RICE, *ibid.* **72** (1989) 2364.
5. D. P. H. HASSELMAN, K. Y. DONALDSON, E. M. ANDERSON and T. A. JOHNSON, *ibid.* **76** (1993) 2180.
6. P. STINGL, J. HEINRICH and J. HUBER in Proceedings of the 2nd International Symposium on Ceramic Materials and Components for Engines, Lübeck-Travemünde, Germany, April 1986, edited by W. Bunk and H. Hausner, (DKG, Bad Honnef, 1986) p. 369.
7. H. MORISHIMA, Z. KATO, K. UEMATSU, K. SAITO, T. YANO and N. OOTSUKA, *J. Mater. Sci. Lett.* **6** (1987) 389.
8. F. J. PARKER, *J. Amer. Ceram. Soc.* **73** (1990) 929.
9. H. WOHLFROMM, J. S. MOYA and P. PENA, *J. Mater. Sci.* **25** (1990) 3753.
10. E. KATO, K. DAIMON and J. TAKAHASHI, *J. Amer. Ceram. Soc.* **63** (1980) 355.
11. M. ISHITSUKA, T. SATO, T. ENDO and M. SHIMADA, *ibid.* **70** (1987) 69.
12. G. TILLOCA, *J. Mater. Sci.* **26** (1991) 2809.
13. T. KAMEYAMA and T. YAMAGUCHI, *J. Ceram. Soc. Jpn.* **84** (1976) 589.
14. E. KATO, K. DAIMON and Y. KOBAYASHI, *ibid.* **86** (1978) 626.
15. V. BUSCAGLIA, G. BATTILANA, M. LEONI and P. NANNI, *J. Mater. Sci.* **31** (1996) 5009.
16. D. B. WILES and R. A. YOUNG, *J. Appl. Cryst.* **14** (1981) 149.
17. E. M. LEVIN and H. F. Mc MURDIE, "Phase diagrams for ceramists, 1975 supplement," (The American Ceramic Society, Columbus, OH, 1975).
18. O. KNACKE, O. KUBASCHEWSKI and K. HESSELMANN, "Thermochemical properties of inorganic substances", (Springer, Berlin, 1991).
19. B. FREUDENBERG and A. MOCELLIN, *J. Amer. Ceram. Soc.* **71** (1988) 22.
20. V. BUSCAGLIA, M. ALVAZZI DELFRATE, M. LEONI, C. BOTTINO and P. NANNI, *J. Mater. Sci.* **31** (1996) 1715.
21. V. BUSCAGLIA, M. ALVAZZI DELFRATE, P. NANNI, M. LEONI and C. BOTTINO, in Proceedings of the 8th CIMTEC (World Ceramic Congress), Firenze, Italy, 28 June–4 July 1994, edited by P. Vincenzini, (Faenza Editrice, Faenza, 1995) p. 1867.
22. Y. OHYA and Z. NAKAGAWA, *J. Mater. Sci.* **31** (1996) 1555.
23. Y. OHYA, Y. TAKAHASHI and Z. NAKAGAWA, *ibid.* **31** (1996) 1361.

Received 11 July 1996
and accepted 17 June 1997